
Optogenetic Deep Brain Stimulation



Group 7:

Dana SHAYAKHMETOVA (NX)

Alex GOLAB (NX)

Daniel Abraham ELMALEH (MT)

Pierre VINET (RO)

1 Summary

The device developed by our team uses optogenetic technology to advance deep brain stimulation therapy for Parkinson's disease:

To enable neurons to respond to light at the high frequencies required for DBS, we selected a rapid-fired Crimson opsin. Light will be delivered through a flexible fiber optic cable with a PDMS core and PVA/PAA cladding. Two Platinum-Iridium electrodes are integrated into the hybrid probe to record LFPs from the target brain area. This configuration enables a controlled closed-loop system to record and stimulate simultaneously with millisecond-level precision.

Moreover, we used biocompatible materials, including the already mentioned platinum-iridium for the electrodes and PDMS for the fiber-optic cables to ensure safety and effective signal transmission. More specifically, these materials were chosen to minimize tissue damage, inflammation, and immune responses supported by prior research.

The electronics design is based on existing deep brain stimulation (DBS) devices. It includes signal amplifiers and mixed-signal filtering located near the implanted electrode site on top of the skull while the Atmel ATTiny 44A microcontroller is implanted below the collarbone, similar to a typical pulse generator in a DBS system. This general design has already been tested and approved in previous DBS models, simplifying long-term use and reliability.

Furthermore, we present a detailed description of the system's architecture, beginning with a block diagram and its purpose. We also outline the fabrication process, focusing on the integration of fiber optics, light delivery systems, and their connection to the neural interface and electronic components. We also address key electrical and mechanical considerations, such as power requirements, electrochemical characterization, and feasibility assessments.

Looking ahead, while our primary focus has been on Parkinson's disease, this approach has the potential for treating other neurological and psychiatric disorders, such as depression and Tourette syndrome. However, advancing this technology to clinical applications will require further research, particularly in the refinement of gene modification techniques for opsin delivery. It is important to note that, as of now, no optogenetic DBS design has been approved by the FDA or any other regulatory authority.

2 State-of-the-art review

2.1 Deep Brain Stimulation

Deep Brain Stimulation (DBS) is a neurosurgical technique delivering high-frequency (>120 Hz) electrical impulses to deep brain structures, such as the subthalamic nucleus and globus pallidus, to modulate neural activity, suppressing pathological patterns and restoring functional networks [1]. This technique has proven highly effective in alleviating motor symptoms of conditions like Parkinson's disease, essential tremor, and epilepsy, and has been approved by the U.S. FDA for clinical use. Additionally, DBS is currently being investigated as a potential treatment for psychiatric disorders, including depression and obsessive-compulsive disorder [2].

Building upon this foundation, recent advancements in closed-loop DBS systems represent a significant step forward. Unlike traditional DBS, which delivers continuous stimulation, closed-loop systems adjust stimulation parameters in real-time based on neural feedback. This dynamic approach improves efficiency, reduces side effects, and prolongs battery life [3].

2.1.1 FDA-Approved DBS Devices

The typical design of a DBS device consists of three main components: a DBS electrode, an Implanted Pulse Generator (IPG), and an insulated wire connecting the two. The DBS electrode is permanently implanted in the target area of the brain, while the wire links it to the IPG, which is placed beneath the collarbone. After implantation, an external programmer is used to adjust the device, controlling the delivery of electrical signals to specific brain regions.

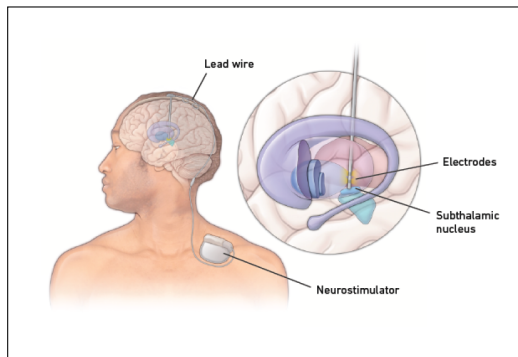


Figure 1: Typical DBS Device Components

Several DBS devices have been FDA-approved for clinical use, most of which are open-loop systems. The first, Medtronic's Activa, was approved in 2002, followed by Abbott's Infinity in 2016 and Boston Scientific's Vercise in 2017. These devices differ in design features, such as the ability to provide directional stimulation for more targeted therapy and options for rechargeable or non-rechargeable batteries, allowing clinicians to tailor treatment for each patient. Furthermore, closest to a closed-loop device is Medtronic's Percept RC which was approved in 2024. While it stimulates the target brain area like other devices, it is the first approved device capable of recording local field potentials from the same area, storing the data for analysis, and allowing professionals to manually adjust the stimulation. Thus, there exist a variety of DBS devices for Parkinson's symptoms but with several limitations.

2.1.2 Areas for Improvement in DBS

Despite the remarkable advancements in DBS, there is still room for improvement in the precision of targeting dysfunctional neuronal populations. One key area of focus is minimizing the spread of electrical current beyond the intended brain regions. For example, a study by Kim et al. (2021) involving 93 patients with 115 implanted DBS electrodes revealed that while the target areas for stimulation were the ventralis intermedius nucleus of the thalamus and the posterior subthalamic area, the electrical current often extended beyond these regions [4]. This led to side effects such as dysarthria, paresthesia, and gait disturbances in several patients.

2.2 Optogenetic Deep Brain Stimulation

Optogenetics is a new technique that combines genetic and optical methods to control the activity of specific neurons with light. This approach involves introducing opsins —light-sensitive proteins— into neurons via viral vectors, making them responsive to specific wavelengths of light. By using it with closed-loop DBS systems, we can selectively target specific cell types, and minimize off-target effects mentioned in the previous section. Thus, the new level of specificity can help ameliorate DBS and improve its therapeutic outcomes. For instance, studies in Parkinsonian animal models have shown that optogenetically stimulating excitatory pathways in the basal ganglia can help restore motor function, and it avoids the side effects commonly seen with conventional DBS [5]

2.2.1 Types of Opsins

Several opsins can be used in optogenetic DBS devices, each chosen based on the desired light frequency and intended effect on neural activity [6]. For example, Channelrhodopsin-2 (ChR2), a blue light-sensitive opsin, is commonly used to excite neurons, while halorhodopsin, activated by yellow light, is used for inhibiting neural activity. Additionally, Chrimson Y261F, a red-shifted opsin, has become a significant advancement due to its ability to penetrate deeper tissues with minimal photodamage [7]. Several Chrimson Y261F opsins have the additional benefit of high-frequency (>150 Hz) responses making this opsin particularly well-suited for in vivo DBS applications, offering improved precision in stimulating specific neural populations.

2.2.2 Light Delivery Methods

Several methods can be used to deliver light in optogenetic deep brain stimulation. One example is the use of μ LEDs integrated into microelectrode arrays (MEAs), which offer miniaturized, high-precision light delivery to specific brain areas. Their small size, efficiency, and ease of integration allow for more localized and effective neuromodulation [8]. Another commonly used approach involves optical fibers, which are known for their flexibility and ability to target specific regions of the brain with great precision. These fibers are often made from fused silica, which minimizes light loss and allows for smaller diameters, reducing the invasiveness of the procedure [9].

The image below illustrates various other approaches that combine electrical recording with optical stimulation.

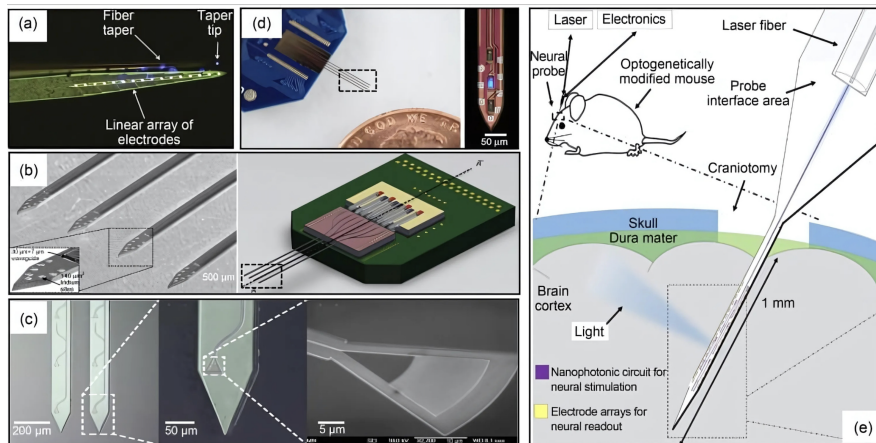


Figure 2: Examples of MEA probes with integrated optical stimulation methods: (a) tapered optical fiber (b) multi-shank electrodes with waveguides (c) photolithographically formed dielectric waveguide (d) neural probe with 32 microLEDs, and (e) scalable probe combining laser fiber and recording.

2.2.3 Drawbacks of Optogenetics

Despite its potential, optogenetics faces significant challenges in clinical application and has not yet been approved for human use in any country. One major hurdle is that the expression of opsins requires genetic modification, which raises ethical and safety concerns [10].

3 Closed-loop Optogenetic Device

3.1 System design

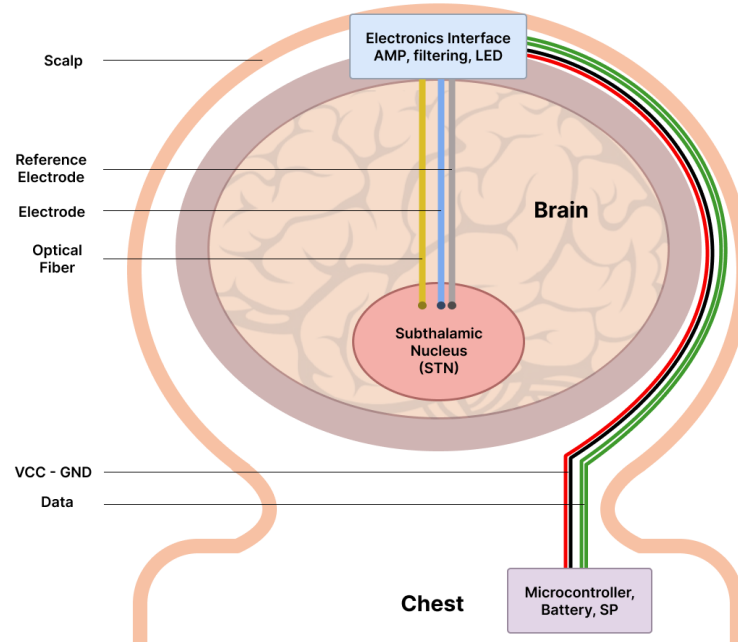


Figure 3: Block diagram of the entire system proposed

Our entire system, illustrated in Figure 3, is designed to record neural activity in the subthalamic nucleus (STN) and to stimulate that same region, functioning as a closed-loop device. The electronics are separated into two parts: one placed between the scalp and the skull, namely the meninges, and the other placed under the skin at chest level.

At the STN region in the brain, the tip of an optical fiber and two electrodes are positioned. The optical fiber delivers light to stimulate the STN, meanwhile, the electrodes record neural activity: one electrode serves as the reference, and the other as the working electrode.

The recorded signal is amplified and filtered as close to the recording site as possible, by the interface electronics at the skull level, to minimize signal loss. This processed signal is then sent via wires to the electronics unit located at chest level, where a microcontroller (MCU) and battery are housed. There, the MCU processes the signal and generates a corresponding PWM output.

This PWM output is sent back to the skull-level electronics, where a LED is activated. The light from this LED is coupled into the optical fiber and transmitted down to the STN region. Because this region has been genetically modified to express opsin proteins, the delivered light can effectively stimulate the targeted neurons.

3.2 Fabrication process flow

3.2.1 Lead

First the PDMS prepolymer (Sylgard 184) will be mixed in a 10:1 weight ratio of prepolymer to curing agent. The mixture will be degassed under vacuum at room temperature to remove excess air from the mixture. After PDMS preparation a glass tube will be inserted into the mixture and then slowly pulled upward through a circular furnace at 280 °C to create the PDMS fiber core. The diameter of the PDMS fiber can be controlled by the speed of the upward pull. The PDMS core will then be treated with oxygen plasma to enhance its adhesion to the cladding. Finally, a thin layer of PVA/PAA will be coated onto the PDMS core through dip coating to serve as cladding. [11] (Figure 4)

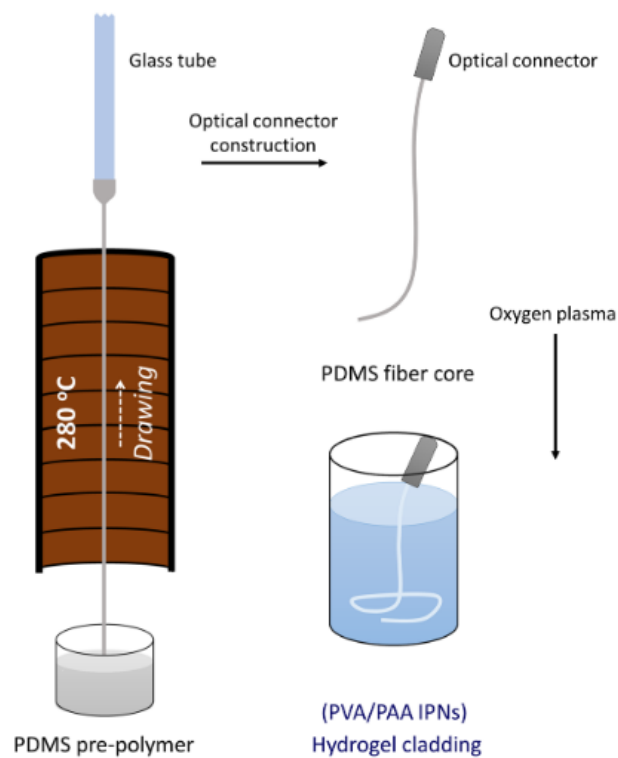


Figure 4: Outline of the fabrication process of the optical fiber [11]

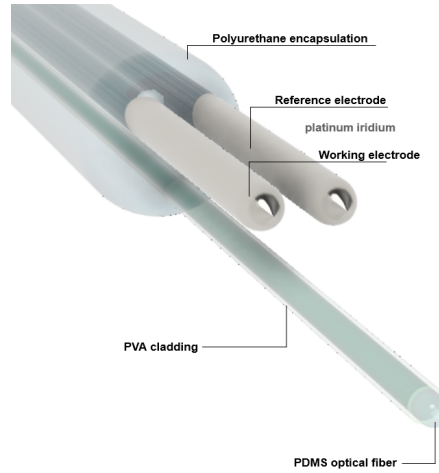


Figure 5: 3D CAD and description of the probe

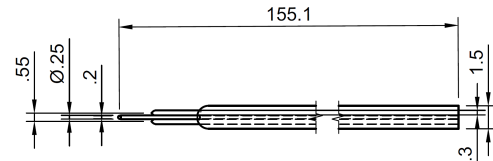


Figure 6: 2D probe dimensions

After fabrication of the optic fiber and the platinum-iridium lead wires, will be placed inside a mold into which Pellethane 2363-80A will be injected. The Pellethane 2363-80A will be injected at 210 °C and left to cure for 16 hours. [12]

In Figure 5 we can see the 3D configuration of the 2 electrodes (PtIr), as well as the optical fiber (PDMS) and its cladding (PVA), and the overall encapsulation in Polyurethane. The optical fiber is longer so to reduce the light propagation blocking by the electrodes. The 2D drawing and dimensions of the probe can be found in Figure 6.

3.2.2 Subdural Device Encapsulation

Part of the DBS device is positioned beneath the patient's scalp. At this stage, the device handles signal amplification and LED driving, necessitating robust encapsulation to protect the electronics from bodily fluids and mechanical stresses.

Platinum is commonly used for burr hole coverings and encapsulation due to its exceptional biocompatibility and corrosion resistance. The housing is typically fabricated using CNC machining to achieve precise dimensions, allowing it to accommodate the electronics securely. Once assembled, the housing is laser-welded shut, ensuring protection from moisture and bodily fluids. [13]

3.3 Electrochemical Characterization

Our electrode will be made of Platinum-Iridium (PtIr) alloy, a material widely used in neural applications for its excellent biocompatibility, mechanical strength, and resistance to corrosion in biological environments [14].

Compared to pure platinum, PtIr exhibits lower impedance, which enhances its performance in neural interfaces [15]. For instance, studies show that platinum electrodes with diameters ranging from 1000 µm to 2.5 µm have impedance values between 1.9 kΩ and 9.0 MΩ [16]. Our electrodes, with diameters between 25 and 50 micrometers, will offer even better performance due to their smaller size and the advantageous properties of PtIr.

While our device uses only recording electrodes, it is useful to look at the electrochemical performance for potential stimulation applications. PtIr offers an improved charge injection capacity (CIC) compared to pure platinum. More specifically, at a PtIr atomic ratio of 55:45, the alloy achieves a charge storage capacity of 22 mC/cm^2 , which surpasses that of pure platinum (16 mC/cm^2). Moreover, long-term cyclic voltammetry studies have shown that PtIr electrodes can undergo activation, increasing their CSC to 29 mC/cm^2 [17].

Platinum-iridium is the preferred material for deep brain stimulation (DBS) electrodes due to these advantages. For instance, Medtronic's latest DBS systems, such as the Percept PC and Activa PC, also use PtIr electrodes, underscoring their reliability in clinical settings [18].

3.4 Mechanical Characterization

3.4.1 Lead

The lead consists of two platinum-iridium (PtIr) electrodes and a fiber optic element at its center. Due to the significantly higher Young's modulus of PtIr (approximately 300 GPa) compared with that of PDMS (1.22 MPa at a 10:1 prepolymer-to-curing-agent ratio) and Pellethane 2363-80A (23.4 MPa), the presence of PtIr conductors largely determines the bending stiffness of the overall structure.

The neutral plane of the probe is located 0.3 mm above its geometric center (Appendix 7.2.1), ensuring that the PtIr wires lie close to this neutral axis, thereby experiencing minimal strain during flexing. This mechanical configuration, combined with the advantageous electrochemical properties of PtIr, ensures durability and reliability when implanted and subjected to physiological motions.

3.5 Electronic Integration

Deep brain recording captures signals in a targeted brain area, using an electrode to analyze brain activity. In order to stimulate at the right time, the right way, a closed-loop system is needed. Our system, designed for deep brain stimulation and reading, aims for the smoothest integration into the patient skull. The core challenge involved combining deep brain electrode, real-time data processing, and a lightweight, rechargeable electronic system. We abstracted the most amount of hardware from the skull to be placed and attached to the T-shirt of the patient. Therefore the electronics and battery are interchangeable and upgradeable easily [19].

3.5.1 Overview of Electronic System Architecture

A detailed view of the electronic system architecture is illustrated in Figure 7, which outlines the signal processing pathway for the reading to the light generation. We will breakdown each of its building blocks in the following sections.

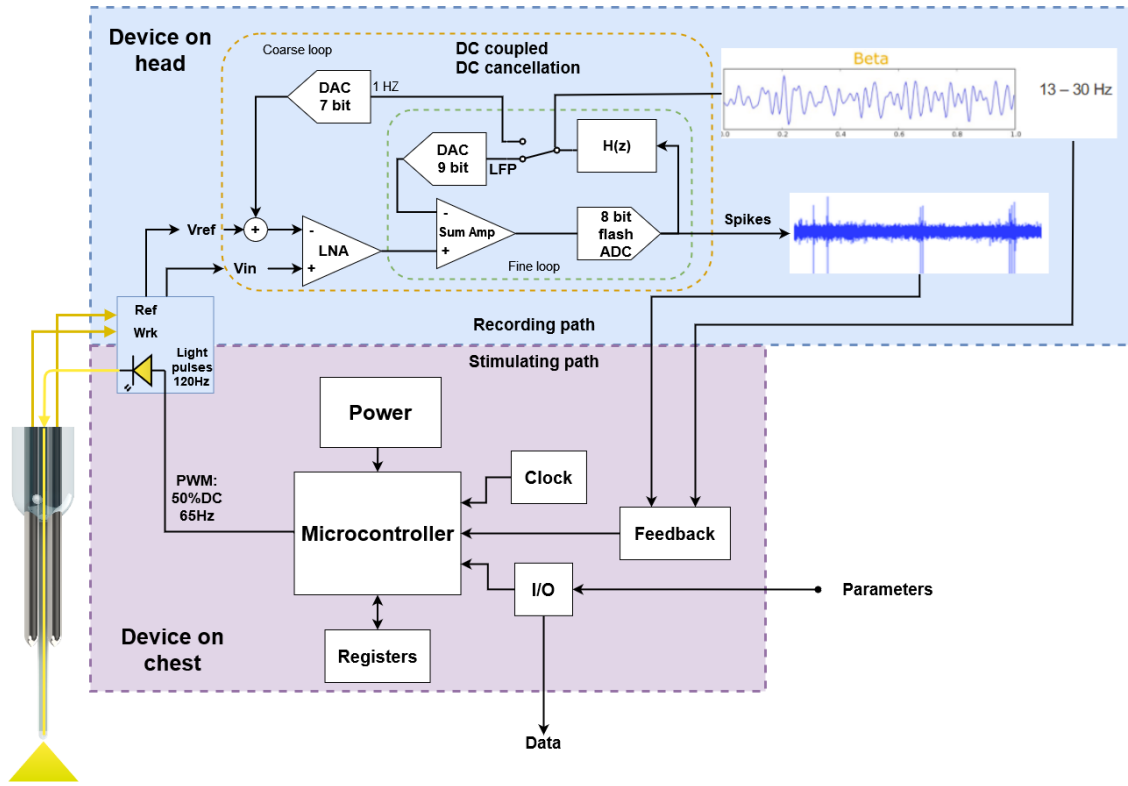


Figure 7: Electrical diagram

3.5.2 Circuit Architecture, Amplification & Filtering

The neural recording interface is designed to capture both low-frequency potentials (LFPs) and high-frequency spike signals from the brain's electrical activity. The input signal V_{IN} may contain offsets of the order of tens of millivolts (mV) due to electrode properties. For instance, open-circuit potentials can reach hundreds of millivolts, but an on-chip resistor with a large value (e.g., several hundreds of $M\Omega$) attenuates a 1 V offset down to approximately 30 mV at the chip input. This arrangement also limits the DC current to around 15 pA, reducing the risk of electrolysis at the electrode-tissue interface.

To handle these offsets and avoid saturation, the system employs a mixed signal dual-loop cancellation scheme [20]. The first (coarse) loop uses a 7-bit Digital-to-Analog Converter (DAC) to reduce a 50 mV offset down to about 1 mV. After this coarse cancellation, a second (fine) loop uses a 9-bit DAC to further reduce the remaining offset and remove the LFP components, effectively isolating the spike signals of interest. By doing so, the total noise floor—assumed around $5 \mu V_{rms}$ —remains well below the quantization noise introduced by the digital correction loops. This dual-loop architecture enables the required 16-bit equivalent resolution without implementing a single, very high-resolution DAC. The coarse loop operates at low frequencies and relatively low resolution in contrast with the fine loop, which makes the extraction of both LFPs and spikes simultaneously possible.

Another key design choice is the shift from classical analog filtering (e.g., large capacitors for low-pass filtering) to digital signal processing. Traditional analog filters require large on-chip capacitors to achieve low cutoff frequencies, increasing both area and mass. Such bulky components are not ideal for implant, where minimizing size and weight is critical. Instead, by digitizing signals as early as possible, the LFP and spike bands are separated and processed digitally with programmable filter characteristics. This digital approach substantially reduces the need for large passive components, leading to a smaller and lighter implant without sacrificing performance. As a result, the entire acquisition chain becomes more efficient, flexible, and easier to integrate into compact implantable devices.

The combined low-noise amplifier (LNA), band-pass filter (BPF), and analog-to-digital converter (ADC) require a total power consumption of approximately $5.04 \mu W$, all operating from a low supply voltage of 0.5 V. The measured common-mode rejection ratio (CMRR) is about 75 dB, indicating effective suppression

of common-mode interference. For noise performance, the input-referred noise at the spike band is around $4.9 \mu\text{V}$, and for the low-frequency potentials (LFP), the IRNoise is about $4.3 \mu\text{V}$. The integrated design occupies a compact silicon area of 0.013 mm^2 in a 65 nm process, ensuring that the entire acquisition chain (LNA, BPF, and ADC) can be efficiently embedded in an implantable device [20].

3.5.3 Microcontroller Unit (MCU)

The device uses an Atmel ATTiny 44A microcontroller. This pico-power 8-bit microcontroller delivers high performance and includes 4 KB of flash program memory, 256B of data SRAM, 256B of EEPROM, 12 general-purpose I/O pins, an 8-bit timer/counter, a 16-bit timer/counter, both internal and external interrupts, an 8-channel 10-bit A/D converter, a programmable watchdog timer, a built-in calibrated oscillator, and four modes for power saving [19]. The microcontroller functions with a voltage source between 1.8 and 5.5 V. Its program memory allows for in-system reprogramming via an SPI serial interface.

The device operates on a 5 V 300 mAh Lithium Ion Polymer battery.

4 Optics

The volume we need to illuminate is approx $3x5x12 \text{ mm}^3$. The power required to activate optogenetic proteins is $0.37\text{--}1.27 \text{ mW/mm}^3$ [21] [7]. The wavelength of our light for stimulation will be 594 nm [7]

The calculations used below are used to determine the optical power transmitted through a PDMS optical fiber with PVA cladding. The calculations account for LED coupling efficiency, fiber transmission losses, numerical aperture, illumination at a distance as well as attenuation in brain tissue.

The following are the main parameters and their typical values for a PDMS fiber with PVA cladding and experimental refractive index for brain tissue:

- Optical power emitted by the LED: $P_{\text{LED}} = 300 \text{ mW}$ [22]
- Coupling efficiency of light: $\eta_{\text{coupling}} = 0.7$ (arbitrarily low for non optimized setup)
- Refractive indices: $n_{\text{core}} = 1.41$, $n_{\text{cladding}} = 1.33$, with $\text{NA} = \sqrt{1.41^2 - 1.33^2} \approx 0.57$
- Fiber properties: Length $L = 15 \text{ cm}$, attenuation coefficient $\alpha_{\text{fiber}} = 0.3 \text{ dB/cm}$
- Brain tissue refractive index: $n_{\text{brain}} = 1.35$ ([23])
- Distance from fiber tip: d (mm)

The numerical aperture (NA) determines the acceptance angle of the fiber, given by $\text{NA} = \sqrt{n_{\text{core}}^2 - n_{\text{cladding}}^2}$. The power coupled to the fiber is $P_{\text{fiber}} = P_{\text{LED}} \times \eta_{\text{coupling}}$, and the power transmitted after losses is $P_{\text{out}} = P_{\text{fiber}} \times 10^{-\alpha_{\text{fiber}} \cdot L/10}$.

The exit half-angle (θ) relates NA and the brain refractive index (n_{brain}): $\theta = \arcsin\left(\frac{\text{NA}}{n_{\text{brain}}}\right)$. The illuminated area (A) at distance d is approximated as

$$A = 2\pi d^2(1 - \cos(\theta)) = 2\pi d^2 \left(1 - \sqrt{1 - \left(\frac{\text{NA}}{n_{\text{brain}}}\right)^2}\right).$$

Finally, the illuminance (output power per unit area) is

$$I = \frac{P_{\text{out}}}{A} = \frac{P_{\text{out}}}{2\pi d^2 \left(1 - \sqrt{1 - \left(\frac{\text{NA}}{n_{\text{brain}}}\right)^2}\right)}.$$

Attenuation in Brain Tissue: $P_{\text{attenuated}} = P_{\text{out}} \cdot \text{Attenuation}$, where *Attenuation* is fitted to the curve of 594 nm from [Figure 10].

The power per unit area after attenuation becomes:

$$I_{\text{tissue}} = \frac{P_{\text{attenuated}}}{A} = \frac{P_{\text{out}} \cdot \text{Attenuation}}{2\pi d^2 \left(1 - \sqrt{1 - \left(\frac{\text{NA}}{n_{\text{brain}}}\right)^2}\right)}. \quad (4.1)$$

The maximum distance satisfying both the minimum power requirement (0.37 mW/mm^2) and the limiting power (10 mW/mm^2) to avoid photochemical damage can be achieved with a duty cycle of 1/7.5 for the PWM signal sent from the MCU to drive the LED. This transforms the 300 mW input to 10 mW at the exit of the fiber. At 1 mm from the fiber tip, we can approximate a division by 100 of the tip output power based on Figure 10. Using Equation 4.1, this results in 0.17 mW/mm^2 , which is below the threshold of 0.37 mW/mm^2 .

Numerical Result: $d = 0.6 \text{ mm}$

Experimental validation is required to confirm that real-world performance aligns with these theoretical predictions. These calculations reveal a significant constraint: with the current architecture, multiple fibers at different depths would be necessary to achieve homogeneous stimulation across the target volume.

Finally, safety and light intensity distribution involve a trade-off between three limiting factors: the maximum power to avoid damage, the minimum power for effective stimulation, and brain absorption, which attenuates light power.

4.1 Coupling Using a Detachable Technique

In this application, a detachable coupling technique is considered to link the micro-LED source to the PDMS optical fiber. This method offers flexibility during assembly and maintenance. A common approach involves using precision ferrules or miniature connectors to align the fiber's core with the LED's emission profile. Such connectors ensure repeatable alignment and minimize optical losses. To further improve coupling efficiency, microlenses can be integrated at the LED or fiber interface to focus the emitted light into the fiber's numerical aperture (NA). An index-matched, biocompatible gel or epoxy may be applied to reduce Fresnel losses at the interface. Although detachable techniques introduce the risk of alignment drift over time, they are particularly useful during prototyping or for systems requiring periodic replacement of components.

5 Feasibility Assessment

5.1 Limitations of Traditional DBS

DBS targeting the Subthalamic Nucleus (STN) traditionally relies on high-frequency ($>150 \text{ Hz}$) electrical current to modulate neuronal activity. While clinically effective, this approach has significant limitations, such as off-target effects and the inability to precisely target specific neuronal populations [25].

5.2 Technical Feasibility

The implementation of an optogenetic DBS system would represent a significant advantage over traditional DBS, which cannot discriminate between different types of neurons. At the core of this approach is the delivery of light-sensitive proteins, or opsins, to the neurons of the STN. Although optogenetics has not yet been fully approved for any clinical treatment, early-phase clinical trials exploring its potential are currently underway [26] which leveraged an adeno-associated virus (AAV) as a delivery vector. By leveraging cell-specific promoters, such as CAMKII α for excitatory neurons, the opsin expression can be limited to the desired neuronal subtypes, ensuring precise modulation. Additionally, the high frequency of stimulation for DBS can be achieved with optogenetics using a Crimson Y261F variant that has shown capability of frequency $>150 \text{ Hz}$ [7]. With this opsin we would be able to reliably excite action potentials in the target neurons required for effective deep brain stimulation.

Light delivery to the STN presents another technical challenge. Due to the depth of the target structure and the light-scattering properties of brain tissue, achieving sufficient illumination without causing heat damage is critical. Fiber optic based approaches have also shown efficacy in being able to deliver sufficient light to an



Figure 8: Illustration of the illumination volume

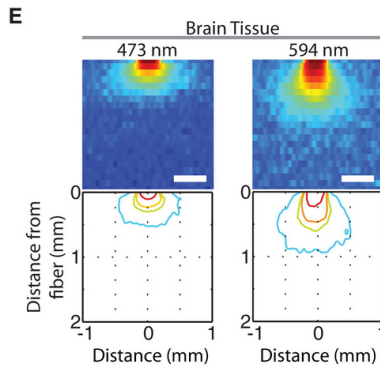


Figure 9: Light propagation in the brain [24]

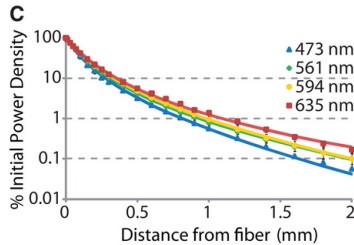


Figure 10: Light power attenuation in brain [24]

optogenetic target while also minimizing the heating during stimulation [11]. Studies have shown that brain co-implantation of electrodes and optic fibers is successfully achievable [19]. For Example, applying these probes in the subthalamic nucleus has helped Parkinsonian rats improve their motor function, like reducing their circling bias and increasing the use of their impaired forelimbs [27].

Finally, regulatory approval would involve oversight from agencies such as the FDA in the United States or the EMA in Europe. The approval process for such devices typically includes preclinical testing, submission of an Investigational Device Exemption (IDE) application, and multiple phases of clinical trials to ensure comprehensive evaluation of risks and benefits. Ethical considerations would require approval from Institutional Review Boards (IRBs) or Ethics Committees to ensure patient safety and compliance with ethical research standards. The use of AAV vectors must adhere to stringent gene therapy regulations to prevent adverse immune reactions or off-target effects.

5.3 Device Usability

The proposed optogenetic DBS device has been designed to align closely with the established shape, size, and physical characteristics of traditional DBS implants. This similarity ensures that its implantation procedure would follow existing clinical workflows, which are already proven to have long-term efficacy. By maintaining the same implantation location and comparable size, the device would minimize patient adaptation challenges and align with current standards for post-surgical monitoring and care. The fiber-optic probe used in the optogenetic system has been engineered to closely conform to the dimensions and stiffness of traditional DBS electrodes. This design choice ensures that the probe utilizes the current state of the art implantation methods used by current DBS probes to ensure the probe is properly placed in its target location. The probe is encased in Polyurethane, the same material used in traditional DBS devices to ensure long term effects are similar.

The compatibility of the optogenetic probe with traditional DBS electrodes ensures a seamless transition for long-term clinical feasibility. Established protocols for follow-up imaging, such as MRI or CT scans, as well as maintenance procedures like battery replacements, can likely be adapted with minimal modifications. This design approach ensures that patients who are eligible for traditional DBS therapy would also be viable candidates for this optogenetic alternative. Furthermore, the similarities in implantation techniques and

device characteristics reduce the risks associated with introducing a novel device, broadening its clinical applicability and making the solution realistic for widespread adoption.

The primary limitation of our device is the local heating caused by light delivery to the target tissue. This needs to be tested and quantified with a prototype to determine the actual levels. Heating can be minimized through the closed-loop nature of our device, which allows stimulation only when necessary. If heating remains excessive, we can switch to a longer wavelength of light [7] to reduce it further.

6 Conclusion

In summary, our project explores the design and feasibility of combining optogenetics with deep brain stimulation to develop a novel therapeutic device for Parkinson's disease. By integrating a platinum-iridium recording electrode and a PDMS fiber-optic light delivery system into a hybrid probe, our design overcomes several limitations of traditional DBS. The selective targeting capabilities of optogenetics utilized in a closed loop system, offer precise control over neural modulation. Additionally, conforming to already-approved DBS structures promises more reliability and simplifies long-term maintenance.

The technical innovations in our design, particularly the dual-loop cancellation scheme and the integration of digital signal processing, demonstrate significant advances in neural recording and stimulation capabilities. The compact design, with electronics distributed between skull and chest locations, represents a practical solution that balances functionality with patient comfort. Our choice of materials, including PtIr electrodes and PDMS-core optical fibers, reflects careful consideration of both performance requirements and biocompatibility concerns.

However, several challenges remain before this technology can transition to clinical use. Further advancements in gene modification technologies, along with rigorous preclinical and clinical testing, will be crucial for transitioning this technology into everyday use. Despite these challenges, the results of preclinical evaluations in numerous studies are promising, indicating potential for broader applications in neurological and psychiatric disorders such as Tourette's Syndrome and ADHD.

Looking forward, our design provides a foundation for future developments in optogenetic neuromodulation. The modular nature of our system allows for future upgrades and modifications as optogenetic technology continues to evolve. Although our current implementation primarily utilizes Local Field Potentials (LFPs) for feedback control, our hardware is capable of recording high-frequency spike signals through the same electrodes. Future iterations could leverage both LFPs and spike data for more sophisticated neural activity analysis, potentially enabling more precise detection of disease biomarkers and better-targeted stimulation responses.

For the encapsulation if PU proves unsuitable, we could switch to silicone for the insulation layer. This change would allow us to retain the same injection mold used for PU, requiring only adjustments to the silicone's heating temperature. Such flexibility in material selection demonstrates the adaptability of our design approach to meet various manufacturing and biocompatibility requirements.

In conclusion, while significant work remains before clinical implementation, our optogenetic DBS system represents a promising step toward more precise and effective treatments for neurological disorders. The combination of targeted genetic modification, precise optical stimulation, and sophisticated electronic control offers a powerful new approach to neuromodulation therapy. Continued research and development in this direction could lead to transformative treatments for patients suffering from a range of neurological conditions.

7 Appendix

7.1 Team work

Most decisions were taken as a team, through frequent discussions and meetings. Alex focused on material selection, manufacturing methods supervision, and fiber optic fabrication, while Dana conducted an extensive state-of-the-art review and performed electrochemical characterization. Daniel oversaw the electrode specifications and dimensions and designed with Alex the optical stimulation path, while Pierre and Daniel led the electronic design and integration.

Throughout the project, regular team meetings provided a platform for brainstorming, problem-solving, and aligning our efforts toward common goals. This collaborative approach allowed us to leverage each member's expertise, leading to a more thorough and efficient development process.

The team emphasized flexibility, with members contributing beyond their primary responsibilities. This dynamic approach enabled us to fully leverage our collective knowledge and expertise, contributing significantly to the project.

7.2 Probe Calculations

7.2.1 Neutral Plane Calculations

$$\begin{aligned}
 z_n &= \frac{\sum(E_i \cdot h_i \cdot z_i)}{\sum(E_i \cdot h_i)} \\
 &= \frac{E_{Pt-Ir} \cdot h_{Pt-Ir} \cdot z_{Pt-Ir} + E_{PDMS} \cdot h_{PDMS} \cdot z_{PDMS} + E_{PU} \cdot h_{PU} \cdot z_{PU}}{E_{Pt-Ir} \cdot h_{Pt-Ir} + E_{PDMS} \cdot h_{PDMS} + E_{PU} \cdot h_{PU}} \\
 &= \frac{300 \times 10^9 \text{Pa} \cdot 3.3 \times 10^{-4} \text{m} \cdot 3.3 \times 10^{-4} \text{m}}{300 \times 10^9 \cdot 3.3 \times 10^{-4} + 1.22 \times 10^6 \text{Pa} \cdot 2.5 \times 10^{-4} \text{m} + 23.4 \times 10^6 \text{Pa} \cdot 8.4 \times 10^{-4} \text{m}} \\
 &+ \frac{1.22 \times 10^6 \text{Pa} \cdot 2.5 \times 10^{-4} \text{m} \cdot 1.25 \times 10^{-4} \text{m}}{300 \times 10^9 \cdot 3.3 \times 10^{-4} + 1.22 \times 10^6 \text{Pa} \cdot 2.5 \times 10^{-4} \text{m} + 23.4 \times 10^6 \text{Pa} \cdot 8.4 \times 10^{-4} \text{m}} \\
 &+ \frac{23.4 \times 10^6 \cdot 8.4 \times 10^{-4} \cdot 4.2 \times 10^{-4}}{300 \times 10^9 \cdot 3.3 \times 10^{-4} + 1.22 \times 10^6 \text{Pa} \cdot 2.5 \times 10^{-4} \text{m} + 23.4 \times 10^6 \text{Pa} \cdot 8.4 \times 10^{-4} \text{m}} \\
 &= 3.3 \times 10^{-4} \text{m}
 \end{aligned}$$

References

1. KONDABOLU, K.; KOWALSKI, M. M.; ROBERTS, E. A.; HAN, X. Optogenetics and deep brain stimulation neurotechnologies. In: KANTAK, K.; WETTSTEIN, J. (eds.). *Cognitive Enhancement: Handbook of Experimental Pharmacology*. Springer, Cham, 2015, vol. 228, pp. 251–273. Available from DOI: 10.1007/978-3-319-16522-6_15.
2. BENABID, A. L.; CHABARDES, S.; MITROFANIS, J.; POLLAK, P. Deep brain stimulation of the subthalamic nucleus for the treatment of Parkinson's disease. *The Lancet. Neurology*. 2009, vol. 8, no. 1, pp. 67–81. Available from DOI: 10.1016/S1474-4422(08)70291-6.
3. LITTLE, S.; TRIPOLITI, E.; BEUDEL, M.; AL., et. Adaptive deep brain stimulation for Parkinson's disease demonstrates reduced speech side effects compared to conventional stimulation in the acute setting. *Journal of Neurology, Neurosurgery Psychiatry*. 2016, vol. 87, pp. 1388–1389.
4. KIM, M. J.; CHANG, K. W.; PARK, S. H.; CHANG, W. S.; JUNG, H. H.; CHANG, J. W. Stimulation-induced side effects of deep brain stimulation in the ventralis intermedius and posterior subthalamic area for essential tremor. *Frontiers in Neurology*. 2021, vol. 12, p. 678592. Available from DOI: 10.3389/fneur.2021.678592.
5. GRADINARU, V.; MOGRI, M.; THOMPSON, K. R.; HENDERSON, J. M.; DEISSEROTH, K. Optical deconstruction of parkinsonian neural circuitry. *Science*. 2009, vol. 324, no. 5925, pp. 354–359. Available from DOI: 10.1126/science.1167093.
6. ZHANG, Q.; LI, T.; XU, M.; AL., et. Application of optogenetics in neurodegenerative diseases. *Cellular and Molecular Neurobiology*. 2024, vol. 44, p. 57. Available from DOI: 10.1007/s10571-024-01486-1.
7. MAGER, T.; LOPEZ DE LA MORENA, D.; SENN, V.; AL., et. High frequency neural spiking and auditory signaling by ultrafast red-shifted optogenetics. *Nature Communications*. 2018, vol. 9, p. 1750. Available from DOI: 10.1038/s41467-018-04146-3.
8. JIA, Q.; LIU, Y.; LV, S.; WANG, Y.; JIAO, P.; XU, W.; XU, Z.; WANG, M.; CAI, X. Wireless closed-loop deep brain stimulation using microelectrode array probes. *Journal of Zhejiang University. Science. B*. 2024, vol. 25, no. 10, pp. 803–823. Available from DOI: 10.1631/jzus.B2300400.
9. WU, F.; STARK, E.; IM, M.; CHO, I. J.; YOON, E. S.; BUZSÁKI, G.; WISE, K. D.; YOON, E. An implantable neural probe with monolithically integrated dielectric waveguide and recording electrodes for optogenetics applications. *Journal of Neural Engineering*. 2013, vol. 10, no. 5, p. 056012. Available from DOI: 10.1088/1741-2560/10/5/056012.
10. FALTUS, T.; FREISE, J.; FLUCK, C.; ZILLMANN, H. Ethics and regulation of neuronal optogenetics in the European Union. *Pflügers Archiv: European Journal of Physiology*. 2023, vol. 475, no. 12, pp. 1505–1517. Available from DOI: 10.1007/s00424-023-02888-8.
11. CAO, Yi; PAN, Suwan; YAN, Mengying; SUN, Chongyang; HUANG, Jianyu; ZHONG, Cheng; WANG, Liping; YI, Lu. Flexible and stretchable polymer optical fibers for chronic brain and vagus nerve optogenetic stimulations in free-behaving animals. *BMC Biology* [online]. 2021, vol. 19, no. 1, p. 252 [visited on 2024-12-03]. ISSN 1741-7007. Available from DOI: 10.1186/s12915-021-01187-x.
12. KRAUSS, Joachim K.; LIPSMAN, Nir; AZIZ, Tipu; BOUTET, Alexandre; BROWN, Peter; CHANG, Jin Woo; DAVIDSON, Benjamin; GRILL, Warren M.; HARIZ, Marwan I.; HORN, Andreas; SCHULDER, Michael; MAMMIS, Antonios; TASS, Peter A.; VOLKMANN, Jens; LOZANO, Andres M. Technology of deep brain stimulation: current status and future directions. *Nature Reviews Neurology* [online]. 2021, vol. 17, no. 2, pp. 75–87 [visited on 2024-12-08]. ISSN 1759-4758, ISSN 1759-4766. Available from DOI: 10.1038/s41582-020-00426-z.
13. ASENCIO-CORTÉS, Carlos; VILLALBA, Gloria; DE VILALTA, Álex; SERRANO, Laura; ÁLVAREZ-HOLZAPFEL, María Jesús; MONTES-GRACIANO, Guillermo; MÁLAGA, Xavier; MUÑOZ-HERNANDEZ, Fernando; GABARRÓS, Andreu. Safety and Performance of a New Burr Hole Covering Device: Results of the Multicenter COVER Registry. *Journal of Neurological Surgery Part A: Central European Neurosurgery* [online]. 2023, vol. 84, no. 5, pp. 445–454 [visited on 2024-12-19]. ISSN 2193-6315, ISSN 2193-6323. Available from DOI: 10.1055/a-1883-0344.
14. SHAH, D. D.; CARTER, P.; SHIVDASANI, M. N.; FONG, N.; DUAN, W.; ESRAFILZADEH, D.; POOLE-WARREN, L. A.; AREGUETA ROBLES, U. A. Deciphering platinum dissolution in neural stimulation electrodes: Electrochemistry or biology? *Biomaterials*. 2024, vol. 309, p. 122575. Available from DOI: 10.1016/j.biomaterials.2024.122575.

15. DELLA VALLE, E.; KOO, B.; PATEL, P. R.; WHITSITT, Q.; PURCELL, E. K.; CHESTEK, C. A.; WEILAND, J. D. Electrodeposited platinum iridium enables microstimulation with carbon fiber electrodes. *Frontiers in Nanotechnology*. 2021, vol. 3. Available from DOI: 10.3389/fnano.2021.782883.
16. WANG, A.; JUNG, D.; LEE, D.; WANG, H. Impedance characterization and modeling of subcellular to micro-sized electrodes with varying materials and PEDOT:PSS coating for bioelectrical interfaces. *ACS Applied Electronic Materials*. 2021, vol. 3, no. 12. Available from DOI: 10.1021/acsaelm.1c00687.
17. GANSKE, G.; SLAVCHEVA, E.; OOVEN, A. van; MOKWA, W.; SCHNAKENBERG, U. Sputtered platinum–iridium layers as electrode material for functional electrostimulation. *Thin Solid Films*. 2011, vol. 519, no. 11, pp. 3965–3970. Available from DOI: 10.1016/j.tsf.2011.01.344.
18. MEDTRONIC. *SENSIGHT™ Directional Leads Deep Brain Stimulation (DBS) Directional Lead System*. 2024. Retrieved December 15, 2024, from <https://europe.medtronic.com/xd-en/healthcare-professionals/products/neurological/deep-brain-stimulation-systems/sensight-lead.html>.
19. EDWARD, E. S.; KOUZANI, A. Z. *A Closed-Loop Optogenetic Stimulation Device*. Vol. 9. 2020. Available from DOI: 10.3390/electronics9010096.
20. R. MULLER, S. Gambini; RABAHEY, J. M. A 0.013 mm², 5 μW, DC-Coupled Neural Signal Acquisition IC With 0.5 V Supply. *IEEE J. Solid-State Circuits*. 2012, vol. 47. Available from DOI: 10.1109/JSSC.2011.2163552.
21. WORBE, Y.; YELNIK, J.; LEHÉRICY, S. Basal Ganglia. In: KOOB, George F.; MOAL, Michel Le; THOMPSON, Richard F. (eds.). *Encyclopedia of Behavioral Neuroscience*. Oxford: Academic Press, 2010, pp. 118–126. ISBN 978-0-08-045396-5. Available from DOI: <https://doi.org/10.1016/B978-0-08-045396-5.00170-6>.
22. *Thor labs*. [N.d.]. Available also from: https://www.thorlabs.com/newgroupage9.cfm?objectgroup_id=6071.
23. SUN, Jingjing; LEE, Sung Jin; WU, Lei; SARNTINORANONT, Malisa; XIE, Huikai. Refractive index measurement of acute rat brain tissue slices using optical coherence tomography. *Optics Express*. 2012, vol. 20, no. 2. Available from DOI: 10.1364/OE.20.001084.
24. YIZHAR, Ofer; FENNO, Lief E.; DAVIDSON, Thomas J.; MOGRI, Murtaza; DEISSEROTH, Karl. Optogenetics in Neural Systems. *Neuron*. 2011, vol. 71. Available from DOI: 10.1016/j.neuron.2011.06.004.
25. APPLEBY, Brian S.; DUGGAN, Patrick S.; REGENBERG, Alan; RABINS, Peter V. Psychiatric and neuropsychiatric adverse events associated with deep brain stimulation: A meta-analysis of ten years' experience. *Movement Disorders* [online]. 2007, vol. 22, no. 12, pp. 1722–1728 [visited on 2024-12-03]. ISSN 1531-8257. Available from DOI: 10.1002/mds.21551. eprint: <https://onlinelibrary.wiley.com/doi/pdf/10.1002/mds.21551>
26. SAHEL, José-Alain; BOULANGER-SCEMAMA, Elise; PAGOT, Chloé; ARLEO, Angelo; GALLUPPI, Francesco; MARTEL, Joseph N.; ESPOSTI, Simona Degli; DELAUX, Alexandre; DE SAINT AUBERT, Jean-Baptiste; DE MONTLEAU, Caroline; GUTMAN, Emmanuel; AUDO, Isabelle; DUEBEL, Jens; PICAUD, Serge; DALKARA, Deniz; BLOUIN, Laure; TAIEL, Magali; ROSKA, Botond. Partial recovery of visual function in a blind patient after optogenetic therapy. *Nature Medicine* [online]. 2021, vol. 27, no. 7, pp. 1223–1229 [visited on 2024-10-10]. ISSN 1078-8956, ISSN 1546-170X. Available from DOI: 10.1038/s41591-021-01351-4.
27. YU, Chunxiu; CASSAR, Isaac R.; SAMBANGI, Jaydeep; GRILL, Warren M. Frequency-Specific Optogenetic Deep Brain Stimulation of Subthalamic Nucleus Improves Parkinsonian Motor Behaviors. *The Journal of Neuroscience* [online]. 2020, vol. 40, no. 22, pp. 4323–4334 [visited on 2024-10-03]. ISSN 0270-6474, ISSN 1529-2401. Available from DOI: 10.1523/JNEUROSCI.3071-19.2020.